REPORT DOCUMENTATION PAGE

Form Approved
OMB No. 0704-0188

1. REPORT DATE *(DD-MM-YYYY)*	2. REPORT TYPE	3. DATES COVERED *(From - To)*
01-07-2010	Journal Article	

4. TITLE AND SUBTITLE

Fine-Scale Volume Heterogeneity in a Mixed Sand/Mud Sediment off Fort Walton Beach, FL

5a. CONTRACT NUMBER

5b. GRANT NUMBER

5c. PROGRAM ELEMENT NUMBER

6. AUTHOR(S)

Kevin B. Briggs, Allen H. Reed, Darrell R. Jackson, and Dajun Tang

5d. PROJECT NUMBER

5e. TASK NUMBER

5f. WORK UNIT NUMBER

74-7632-07

7. PERFORMING ORGANIZATION NAME(S) AND ADDRESS(ES)

Naval Research Laboratory
Marine Geoacoustics Division
Stennis Space Center, MS 39529

8. PERFORMING ORGANIZATION REPORT NUMBER

NRL/JA/7400-08-5

9. SPONSORING/MONITORING AGENCY NAME(S) AND ADDRESS(ES)

Office of Naval Research
800 North Quincy Street
Arlington VA 22217-5000

10. SPONSOR/MONITOR'S ACRONYM(S)

ONR

11. SPONSOR/MONITOR'S REPORT NUMBER(S)

12. DISTRIBUTION/AVAILABILITY STATEMENT

Approved for public release; distribution is unlimited

13. SUPPLEMENTARY NOTES

IEEE Journal of Oceanic Engineering, Vol. 35, No. 3

Abstract—As part of the effort to characterize the acoustic and physical properties of the seafloor during the high-frequency 2004 Sediment Acoustics Experiment (SAX04), fine-scale variability of sediment sound speed and density was measured in a medium quartz sand using diver cores and an *in situ* conductivity probe. This study has a goal of providing environmental input to high-frequency backscatter modeling efforts. Because the experiment was conducted immediately following exposure of the site to Hurricane Ivan, measurements revealed storm-generated sedimentary structure that included mud deposits and trapped sand pockets suspended in the mud. Fluctuations of sediment sound speed and density were measured downcore at 1- and 2-cm increments, respectively, with standard laboratory techniques. Sediment density was also measured on a very fine scale with an *in situ* conductivity probe [*in situ* measurement of porosity (IMP2)] and by means of computed tomography (CT) imaging of a diver core. Overlap between the locations of the diver cores and the conductivity probe measurements allowed an examination of multiple scales of sediment heterogeneity and a comparison of techniques. Sediment heterogeneity was characterized using estimates of covariance corresponding to an algebraic form for

15. SUBJECT TERMS

Computed tomography (CT), conductivity, heterogeneity, sediment density, sediment sound speed

16. SECURITY CLASSIFICATION OF:			17. LIMITATION OF ABSTRACT	18. NUMBER OF PAGES	19a. NAME OF RESPONSIBLE PERSON
a. REPORT	b. ABSTRACT	c. THIS PAGE			Kevin Briggs
Unclassified	Unclassified	Unclassified	UU	17	19b. TELEPHONE NUMBER *(Include area code)* 228-688-5518

Fine-Scale Volume Heterogeneity in a Mixed Sand/Mud Sediment off Fort Walton Beach, FL

Kevin B. Briggs, Allen H. Reed, Darrell R. Jackson, and Dajun Tang

Abstract—**As part of the effort to characterize the acoustic and physical properties of the seafloor during the high-frequency 2004 Sediment Acoustics Experiment (SAX04), fine-scale variability of sediment sound speed and density was measured in a medium quartz sand using diver cores and an *in situ* conductivity probe. This study has a goal of providing environmental input to high-frequency backscatter modeling efforts. Because the experiment was conducted immediately following exposure of the site to Hurricane Ivan, measurements revealed storm-generated sedimentary structure that included mud deposits and trapped sand pockets suspended in the mud. Fluctuations of sediment sound speed and density were measured downcore at 1- and 2-cm increments, respectively, with standard laboratory techniques. Sediment density was also measured on a very fine scale with an *in situ* conductivity probe [*in situ* measurement of porosity (IMP2)] and by means of computed tomography (CT) imaging of a diver core. Overlap between the locations of the diver cores and the conductivity probe measurements allowed an examination of multiple scales of sediment heterogeneity and a comparison of techniques. Sediment heterogeneity was characterized using estimates of covariance corresponding to an algebraic form for the power spectrum of fluctuations obtained from core, conductivity, and CT measurements. Correcting for sampling brings the power spectra for density fluctuations determined from the various measurements into agreement, and supports description of heterogeneity at the site over a wide range of scales by a power spectrum having a simple algebraic form.**

Index Terms—**Computed tomography (CT), conductivity, heterogeneity, sediment density, sediment sound speed.**

I. Introduction

FIVE years following the 1999 Sediment Acoustics Experiment (SAX99) [1], [2] another high-frequency acoustic sediment experiment sponsored by the U.S. Office of Naval Research was conducted about 1 km inshore from the original site. The 2004 Sediment Acoustics Experiment (SAX04) site was located 1 km offshore of the Florida Panhandle in 16.5 m of water. Chief among the goals of SAX04 was the characterization of sediment heterogeneity, expressed as the variability of acoustic and physical properties in the upper 12–30 cm of sediment and throughout the 0.3×0.3-km^2 site. From fluctuations in values of bulk density, porosity, and sound speed in sediments, the potential for scattering from the sediment volume can be assessed [3, ch. 7, Sec. 7.1]. Moreover, predictions of scattering from the sediment volume using perturbation theory require the determination of the power spectra for density and sound-speed fluctuations from measurements of sediment variability [3, Sec. 7.2]. Such variability must be measured at scales comparable to the acoustic wavelength to quantitatively model the backscattering originating from the sediment heterogeneity.

Before the collection of measurements of sediment heterogeneity, Hurricane Ivan, a category 3 hurricane, came ashore 100 km to the west of the experiment site. Upon retreat of the estimated 10–12-m-high seas and 3–4.5-m storm surge at the experiment site, a significant amount of mud, likely derived from the lagoon north of the barrier island (Santa Rosa Island) was transported onto the shelf, where it formed a continuous-to-quasi-continuous layer. A more thorough account and discussion of the storm stratigraphy is provided by Vaughan *et al.* [4]. Subsequent to the mud drape, wind-wave activity mobilized sediment and some of the mud layer was resuspended, and sand from the storm-generated ripple crests was transported onto the remaining mud layer. Settling of the suspended mud resulted in the formation of sand lenses within the mud drape. Lens-shaped mud inclusions within the sand sediment, or flasers, were created when the mud that settled into the troughs of ripples was covered by migrating sand ripples [5], [6]. The result was that some mud was incorporated into the seafloor sediments and protected from resuspension by bottom currents. Over the course of the experiment, subsequent storm events broke up the surface mud layer into small clasts, which were subsequently isolated and buried by migrating sand [7]. Although this experiment was conducted in a moderately well-sorted, medium quartz sand (mean diameter = 363 μm), the presence of mud layers and lenses created a more heterogeneous sediment than existed before the storm when the site was chosen.

Near-surface sediment heterogeneity at the SAX04 site was measured employing two approaches: collection of diver cores from which sediment sound speed and porosity are determined and *in situ* measurement of sediment porosity by a remotely deployed system [*in situ* measurement of porosity (IMP2)] that uses a mechanically driven conductivity probe [8]. Some of the diver cores were purposely collected in the same location at which IMP2 probe measurements were made. One of the cores collected at the site of IMP2 measurements was scanned with a CT imager with the intention of using the X-ray attenuation data to determine the density of the core sediment at very fine increments (95 μm). The results from the different approaches complement each other and constitute a unique data set composed

Manuscript received May 25, 2008; revised August 05, 2009; accepted September 29, 2009. Date of publication July 26, 2010; date of current version September 01, 2010. This work was supported by the Office of Naval Research (ONR) and Naval Research Laboratory (NRL) Program Element 0601153N. The NRL contribution number is JA/7400-08-0005.

Guest Editor: E. Thorsos.

K. B. Briggs and A. H. Reed are with the Seafloor Sciences Branch, Naval Research Laboratory, Stennis Space Center, MS 39529-5004 USA (e-mail: kbriggs@nrlssc.navy.mil; areed@nrlssc.navy.mil).

D. R. Jackson and D. Tang are with the Applied Physics Laboratory, University of Washington, Seattle, WA 98105 USA (e-mail: drj@apl.washington.edu; djtang@apl.washington.edu).

Digital Object Identifier 10.1109/JOE.2010.2041834

TABLE I
LOCATIONS OF SEAFLOOR-MOUNTED INSTRUMENTATION, DATES ON WHICH THE LOCATIONS WERE SAMPLED BY DIVERS, TOTAL NUMBER OF CORES COLLECTED AT EACH LOCATION, AND DESCRIPTIONS OF INSTRUMENTS INCLUDING THEIR PROVENANCE

Location	Latitude	Longitude	Dates Sampled	Total No. of Cores Collected	Description
Dal 1	30° 23.225'N	86° 38.556'W	21 Sep 2004 12 Oct 2004 31 Oct 2004	5	Dalpod 1 (Dalhousie University)
Dal 2	30° 23.201'N	86° 38.547'W	23 Sep 2004 14 Oct 2004	4	Dalpod 2 (Dalhousie University)
BAMS	30° 23.284'N	86° 38.496'W	29 Sep 2004 30 Sep 2004 3 Oct 2004 13 Oct 2004	7	Benthic Acoustic Measurement System—40 kHz (APL-UW)
XBAMS	30° 23.203'N	86° 38.496'W	2 Oct 2004 14 Oct 2004	4	Benthic Acoustic Measurement System—300 kHz (APL-UW)
SJ	30° 23.24' N	86° 38.64' W	4 Oct 2004 5 Oct 2004 16 Oct 2004 31 Oct 2004	11	R/V Seward Johnson
ARL	30° 23.241'N	86° 38.642'W	13 Oct 2004	4	ARL-UT buried acoustic line array
B'ham	30° 23.150'N	86° 38.601'W	15 Oct 2004	2	Buckingham acoustic sensor station (SIO)
Rail 1	30° 23.221'N	86° 38.660'W	18 Oct 2004 22 Oct 2004 23 Oct 2004	8	Rail Acoustic Tower—1st position (APL-UW)
Rail 2	30° 23.221'N	86° 38.661'W	31 Oct 2004 3 Nov 2004	6	Rail Acoustic Tower—2nd position (APL-UW)
Zimmer	30° 23.24' N	86° 38.64' W	25 Oct 2004	5	Zimmer buried hydro/geophone array (NRL)
DRDC	30° 23.232'N	86° 38.714'W	3 Nov 2004	2	Defence R&D Canada sensor array

of multiple spatial scales of vertical fluctuation of sediment density. These results reported for SAX04 have broader implications for assessment of sediment heterogeneity as a parameter for predicting acoustic scattering from the seafloor than what is necessary for characterizing the SAX04 site. For instance, extrapolation from centimeter-scale to millimeter- or micrometer-scale heterogeneity is evaluated from field sediment data that contains real-world complexity. Moreover, the issue of bias resulting from finite spatial resolution is addressed and examined at the different sampling scales.

II. METHODS

A. Core Data Analysis

During SAX04, 58 diver cores were collected from 11 locations within the study area. These 11 locations coincided with the locations of seafloor-mounted instrumentation (Table I). Each of the 5.9-cm-inside-diameter, polycarbonate plastic, cylindrical cores was used to measure sediment sound speed and attenuation at 400 kHz at 1-cm increments using a pulse technique directly through the core walls [3, Sec. 5.1.1]. Collection, measurement, and handling procedures were designed to minimize sampling disturbance and to maintain an intact sediment–water interface within the core samples.

Twenty three of the 58 cores were sectioned at 2-cm intervals to determine sediment porosity, average grain density, and grain size distribution. Sediment water content was measured by the water-weight loss of sediment dried at 105 °C for 24 hours after transport of the cores to a shore-based laboratory from one to 33 days after collection by divers. Sediment bulk density was later calculated from the fractional porosity calculated from water content and average grain density measured with a pycnometer as described in [8]. Values of grain density averaged 2656 kg · m^{-3} for sand, but only 2479 kg · m^{-3} for mud, probably due to associated organic matter. The accuracy and repeatability of the gravimetric technique were comparable to previous results. As in some previous porosity analyses in sand [3, p. 95], several cores were not sectioned at 2-cm intervals, but assayed whole to determine effects of handling. The difference in average values of fractional porosity between the 23 sectioned cores and the five whole (unsectioned) cores was 0.003 in the SAX04 results.

From the same dried, 2-cm-thick extruded samples weighed for water-weight loss and utilized for grain density measurements, the sediment grain size distribution was determined. Grain size distribution was determined by dry-sieving for sand- and gravel-sized particles and pipettes for the silt/clay fraction [3, pp. 80–81].

Mud layers were subsampled to provide a wet sample for grain size analysis separate from the dried sample used for water content and grain density. Grain size distributions for mud layers were determined with the aid of a Micromeritics Sedigraph III particle size analyzer. The grain size data are used to ascertain sediment volume heterogeneity that may

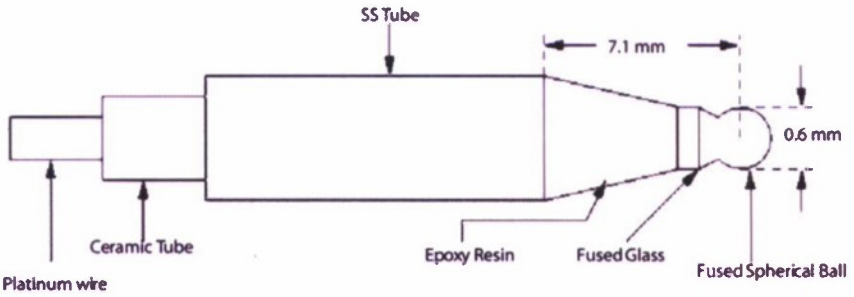

Fig. 1. Resistivity probe used to make porosity measurements [8]. All parts are insulated from the seawater except for the small spherical electrode. This probe is inserted vertically into the sediment in small steps to obtain profiles of resistivity.

result from differences in grain size that could be attributed to patchiness of sediment deposition within the experiment site. As a result of the storm event (Hurricane Ivan), the sand grains were relatively uniformly dispersed in the surficial sediment, but the fine-grained fractions (silt and clay sizes) were relegated to discrete layers, lenses, or clasts, occurring in 45% of all collected cores but occupying only 8.5% of the aggregated volume of all cores.

The power spectral densities (equivalently, correlation functions and variances) for fluctuations in sediment sound speed and bulk density are important model inputs that can be estimated from the core data. For the SAX99 data, parameters for exponential correlation functions were estimated from the core data by using a first-order autoregressive model [8]. Because one object of the present work is to compare heterogeneity measurements obtained by differing methods and having differing spatial resolution, a new approach is used here for SAX04 data [3, Sec. 7.4]. In this approach, the smoothing effect due to sampling resolution is compensated, facilitating comparison of data obtained with resolutions from 2 cm to approximately 0.5 mm. The procedure used here to correct bias due to finite resolution is adapted from [3, Sec. 7.4] and presented in detail in the Appendix. While it produces the largest corrections for the lowest resolution (core) data, it is also applied to the higher resolution data obtained from a conductivity-probe system.

B. Conductivity System

The IMP2 system that was used in SAX04 differed operationally from the IMP array used in SAX99 [8]. Instead of an array of 16 constant-current electrodes, a single, more robust electrode (Fig. 1) was employed by IMP2 in SAX04. A detailed description of this system can be found in [9]. In a typical deployment, IMP2 is placed on the seafloor with diver help in positioning. When started according to a programmed procedure, the electrode is used to take vertical conductivity measurements with 1-mm vertical steps. Data are collected starting 2 cm above the seafloor and to a depth of 10–15 cm into the seafloor. After one vertical measurement is completed, the electrode is lifted up to its starting position in the water, and then a horizontal drive moves the electrode to a new horizontal position, all in 1-cm steps, and another vertical measurement follows. Repeating these steps, a 2-D data set along the seafloor is obtained. From such data, we obtain the formation factor F [8]–[10] and sediment porosity η calculated according to an empirical relation known as "Archie's law" [9]–[11]

$$\eta = \frac{1}{F^{1/m}} \tag{1}$$

where m is a constant for a given sediment material. This constant was determined using averages of the IMP2 formation factor values over the data sets to be discussed below. Assuming an average porosity from Table II of 0.366, (1) is solved to yield $m = 0.92 \pm 0.02$ where the mean and the standard deviation were formed from the three averages. Using $m = 0.92$, the IMP2 formation factor values were converted to porosity, and wet bulk density ρ was obtained as

$$\rho = \eta\rho_w + (1-\eta)\rho_g \tag{2}$$

where $\rho_w = 1024\ \text{kg} \cdot \text{m}^{-3}$ is the nominal density of seawater, and $\rho_g = 2656\ \text{kg} \cdot \text{m}^{-3}$ is the average grain density for SAX04 sand.

C. Computed Tomography Imaging

A high-resolution computed tomography (CT) system was used to collect X-ray images of one diver core that was collected at the same location as an insertion of the IMP2 probe. Following shipboard acoustic logging and transport to the laboratory, the 5.9-cm-inside-diameter core was imaged from the overlying water down to approximately 7.6 cm into the sediment. The CT system is an HD-500 from Universal Systems, Inc. (Solon, OH). This system produced polychromatic X-rays that are projected in a cone beam through the sample, which rotates about the vertical axis, and into the image intensifier. To provide a good flux of X-rays, the CT was operated at high (160 keV and 65 mA) and low (100 keV and 200 mA) energies with a 5-μm focal spot size. The attenuation, or difference between the calibrated X-ray energies that are projected when there is no sample in the X-ray path and those that are projected through the core sample, is then determined for many elevations and along many different angles through the sample. In this way, attenuation may be measured through the entire core sample and integrated over small portions of the core. The attenuation data that form the image are converted to 16-bit grayscale values and these volume elements are called voxels, which are 3-D pixels of cubic form. In this case, the voxels that comprise the 95-μm resolution grayscale image are 95 μm on each edge. Thus, 800 individual CT image "slices" of 16-bit grayscale values were

collected through the top of a sand core to a depth of 7.6 cm. These data are then corrected for beam-hardening effects, which is a common issue with polychromatic energy sources, such as the HD-500 and medical CT systems. Beam hardening is a process that occurs in all polychromatic X-ray systems whereby lower energy, more easily attenuated X-rays are removed from the X-ray energy spectrum after passing into the sample material, in this case the sediment. The result is that the lower energy X-rays do not reach the detector and the energy spectrum shifts towards a more monochromatic spectrum of higher energy, less easily attenuated X-rays.

To determine sediment bulk density from grayscale values, two different approaches were used. For comparison of smoothed CT data with core data, a dual-energy approach was used. In this approach, X-ray scans were made at a high energy of 160 keV to take advantage of the Compton scatter and at a lower energy of 100 keV to take advantage of photoelectric absorption. Calibration was accomplished by scanning, at each energy level, a "standard" core with identical geometry to the diver core, but containing quartz sand from SAX04 and calibrated standards water, Teflon, oil, aluminum for which the density was quantified on a Quantachrome Instruments PentaPycnometer. The grayscale data for objects of known density could then be used to create a standard curve that relates grayscale values to density from which each voxel in an image could be assigned a density. Alternatively, and in this case, the high and low energy scans are combined into a single data file using VoxelCalc software from Kehlco, Inc. (Houston, TX) and the linear attenuation coefficient for each voxel is determined. The linear attenuation coefficient (μ) is related to the bulk density ρ and the atomic number Z in the following equation:

$$\mu = \rho\left(\frac{a + bZ^{3.8}}{E^{3.2}}\right)\text{[12]} \tag{3}$$

where a is the Klein–Nishina coefficient (related to Compton scattering or the higher energy X-rays in the spectrum), b is a constant (related to photoelectric absorption and the lower energy X-rays), and E is the energy used in the respective scans. The calibrated core that contained samples of known density is used to solve for the coefficients in this equation. Upon solving this equation on a voxel-by-voxel basis, images that relate to the bulk density and the atomic number are produced [12]. The bulk density image may then be used to determine density for any voxel or combination of voxels within the sample. For comparison with gravimetrically derived core density results, a large number of voxels were used, with averaging over disks of diameter 3.9 cm in the center of the core with thickness of 95 μm. While chosen to obtain an approximate match to core-sampling resolution, this large averaging volume had the additional benefit of suppressing occasional outliers (spikes) in the CT-determined density. These data will be referred to as "low-resolution CT data."

For comparison of CT imagery and IMP2 conductivity data, much smaller averaging volumes were used, for which outliers could not be suppressed. For this case, a single-energy approach was used, which avoided the outliers evident in the dual-energy approach. A standard grayscale curve was generated for water, oil, and quartz crystals of known density. To ensure that the attenuation data for these standards were useful, the standard sample materials were scanned in the same diameter column as the sand, essentially a laboratory-produced diver core, while they were embedded in quartz sand. This enables accurate comparisons of grayscale values for attenuation for the sand cores with the materials used to compose the standard curve. Then, the equation for a line was determined from the slope of the standard curve, and this equation was applied to the data grayscale values to convert them to density values. Vertical profiles were extracted, again with a restriction to the inner portion and avoiding the upper mud layer. The available profiles were "thinned" by keeping nine sets of closely spaced profiles, each set being composed of 100 profiles in a 10-profile-by-10-profile horizontal square with 0.05-mm spacing between adjacent profiles. The CT sample spacing in the vertical dimension was 0.095 mm, and the vertical extent of each profile was 3.6 cm. This group of 800 profiles will be referred to as "high-resolution CT data." For direct comparison with IMP2 data, these CT data were averaged over rectangular volumes composed of the 100 profiles in each set and over a depth interval of five samples (0.475 mm). This yields a sampling volume (0.5 mm × 0.5 mm × 0.475 mm) comparable to that of IMP2. The CT data treated in this fashion will be referred to as "medium-resolution averaged CT data."

III. Results of Standard Analysis

A. Acoustic and Gravimetric Data

Sediment sound speed (V_P) and attenuation show the most variability in the top 10 cm of sediment (Fig. 2). Low values of V_P correspond to mud layers and flasers. Values of sound speed intermediate to values attributed to mud and sand correspond to mixtures of sand and mud, sometimes occurring as sand lenses within mud. In fact, the interfaces between mud and sand are almost certainly responsible for scattering the 400-kHz sound that contributes to the high values (> 0.4 dB $\cdot$ m$^{-1}\cdot$ kHz^{-1}) of sound-speed attenuation seen in the top 14 cm of sediment. Trends of sound speed and attenuation exclusive of effects from the presence of mud exhibit slight increases as functions of depth. Below about 4 cm, sediment sound speed remains generally constant down to the deepest measurements obtained.

Aside from mud layers and flasers, values of bulk density and mean grain size exhibit little variability as functions of depth in the sediment (Fig. 3). In general, the values of bulk density and the mean of the grain size distributions reflect the same patterns exhibited in the 400-kHz acoustic measurements in Fig. 2, especially in terms of the presence of mud in the top 10 cm of the core sediment. Note in Fig. 3 that some measurements do not fall consistently at 2-cm intervals due to sectioning of the cores to allow extraction of mud layers separate from the surrounding sand.

Restricting the statistical treatment of the core data to only the sand constituents indicates that the poststorm properties of the recently settled sand are quite uniform (Table II). The coefficient of variation (CV) provides a convenient characterization of levels of heterogeneity. The CV is defined as the standard deviation divided by the mean and multiplied by 100. Comparisons of the CV values of Table II with those of other sediments from similar environments show values for sound speed, porosity,

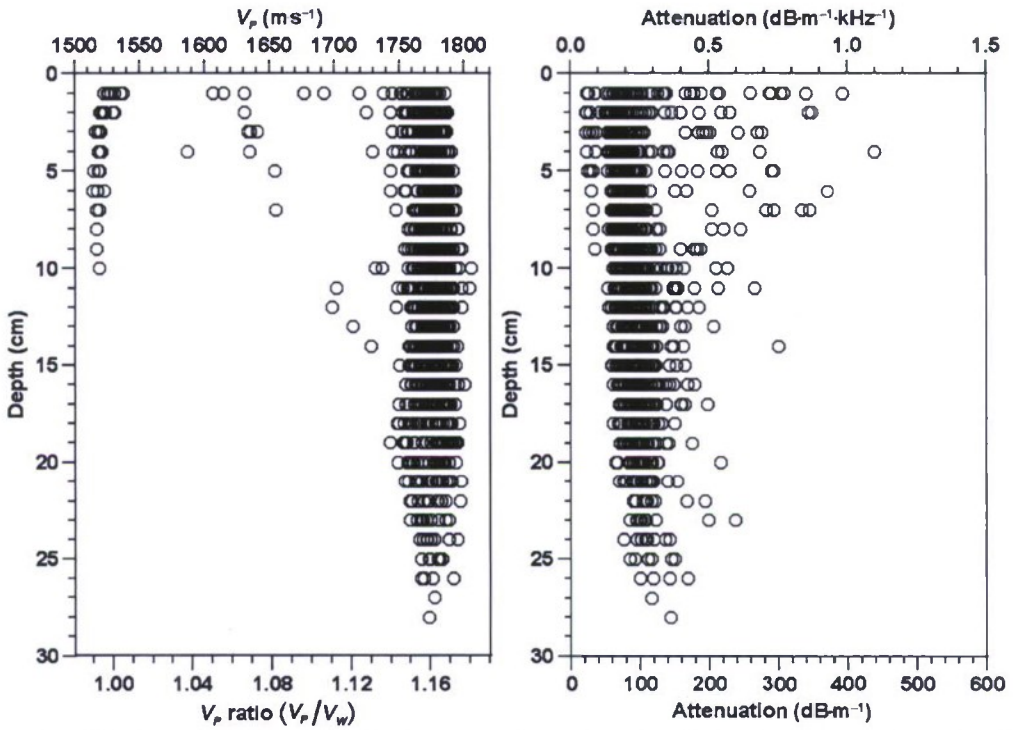

Fig. 2. Sediment sound speed (V_P), sound-speed ratio (V_P/V_W), and attenuation as a function of depth in the sediment as determined from laboratory core analysis. $V_W = 1529$ m · s^{-1}, sound speed in seawater at 23 °C, 35 psu, and 0-m water depth.

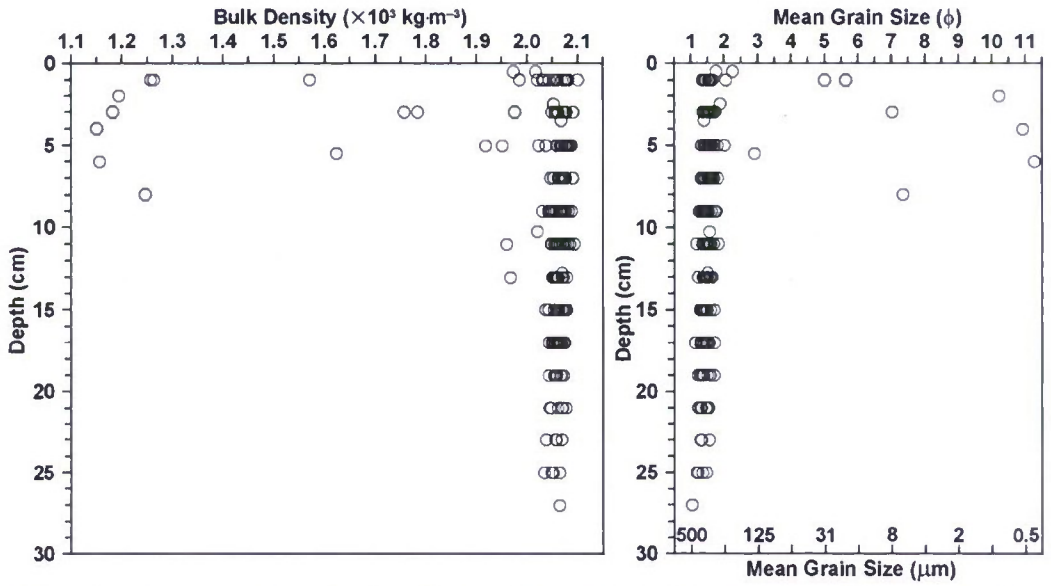

Fig. 3. Sediment bulk density and mean grain size as a function of depth in the sediment for the 23 cores sectioned. Of the 58 cores collected and analyzed for sound speed and attenuation, 23 were also analyzed for bulk density and grain size distribution. Grain size units are given as $\phi = -\log_2$ [dia. in mm] and μm.

bulk density, and mean grain size of the SAX04 sand to be lower than expected for these parameters in medium sands [3, Sec. 7.5.1], [13]. Moreover, there is little apparent variation in sediment bulk density and mean grain size among sites within the SAX04 experiment site when average values and ± 1 standard deviation values of these two parameters in mud-free sand are examined as a function of location (Fig. 4). The average values for these two parameters, indicated by dashed lines in Fig. 4, nearly all fall within the range of variation for each of the 11 locations at which samples were collected during SAX04. The grain size data are more variable (CV for mean grain size is almost 17 times greater than that of bulk density), and thus more locations have averages farther from the site average. As will be seen in the following analysis of finer scale variation (heterogeneity), there is a pronounced spatial variability of more subtle nature in that fluctuation spectra show statistically significant dependence upon measurement location. These heterogeneity spectra are estimated from core measurements of sound speed or core and conductivity measurements of bulk density by using the covariance model presented in the Appendix.

TABLE II
NUMBER OF CORES, AVERAGE VALUE, AND COEFFICIENT OF VARIATION FOR VALUES OF SOUND SPEED, SOUND ATTENUATION, FRACTIONAL POROSITY, BULK DENSITY, AND MEAN GRAIN SIZE FROM SAND, MIXED SAND AND MUD, AND ALL SEDIMENTS. VALUES FOR SAND ARE GATHERED FROM ALL CORES, BUT INTERVALS CONTAINING MUD WERE EXCLUDED. CV IS CALCULATED AS STANDARD DEVIATION ÷ AVERAGE ×100

	Sound Speed ($m \cdot s^{-1}$)	Sound Attenuation ($dB \cdot m^{-1}$)	Fractional Porosity	Bulk Density ($kg \cdot m^{-3}$)	Mean Grain Size (ϕ)
Sand					
No. of cores	58	58	23	23	22
Average	1775.6	91.8	0.366	2064	1.46
CV (%)	0.53	30.15	1.78	0.59	9.43
Sand/Mud[1]					
No. of cores	25	25	14	14	9
Average	1619.7	149.3	0.570	1725	5.09
CV (%)	6.26	73.28	37.43	20.24	72.44
Mud					
No. of cores	8	8	3	3	1
Average	1519.7	30.4	0.885	1212	10.81
CV (%)	0.25	23.26	3.24	4.19	4.96
All					
No. of cores	58	58	23	23	22
Average	1764.4	98.0	0.390	2025	1.70
CV (%)	2.79	46.95	24.77	7.88	75.46

[1]These data correspond to the "Mud" data discussed in [18]. Note: some of the tabulated data in [18] refer to a subset of these data corresponding to specific locations (Rail 1 and Rail 2).

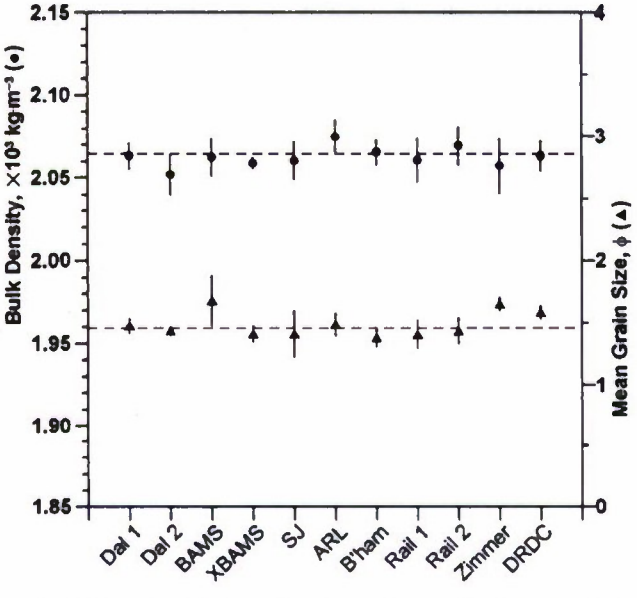

Fig. 4. Sediment bulk density (black dots) in $kg \cdot m^{-3}$ and mean grain size (black triangles) in ϕ units of sand (excluding mud) as a function of location within the SAX04 site (see Table I). Bars are ± 1 standard deviation. Dashed lines are the mud-free SAX04 site averages for density and grain size. Phi (ϕ) units are $-\log_2$(dia. in mm).

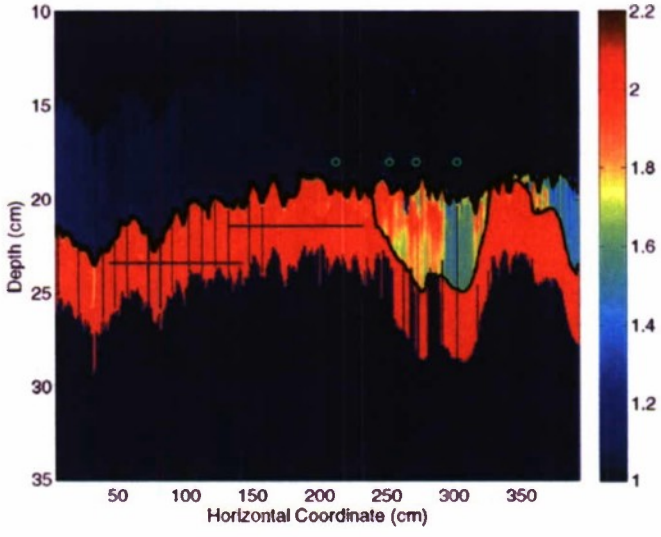

Fig. 5. Wet bulk density as determined from IMP2 run 117, oriented parallel to the ripple strike. There are no data for the highest and lowest dark blue regions. The vertical and horizontal blue lines indicate the data points used in analysis, and the green circles show the locations of diver cores. The vertical line under the right-hand green circle is the centerline of the five IMP2 profiles depicted in the far-right plot of Fig. 8(b). The seafloor and mud/sand interfaces are delineated by black curves. The colorbar units are $kg \cdot m^{-3}$. Depth in the vertical axis is referenced to an arbitrary point on the IMP2 frame.

B. Conductivity Data

Figs. 5 and 6 display data from two IMP2 runs, expressed as wet bulk density using the method outlined in the previous section. Heterogeneity on various scales is evident including mud layers, sand pockets within these layers, and more subtle variations in density on smaller scales. The portions of the IMP2 data to be analyzed are denoted by horizontal and vertical lines in Figs. 5 and 6. The horizontal lines have length 100 cm for run 117 and 40 cm for run 118. The vertical lines of run 117 have length 3.5 cm. These lines were chosen in an attempt to isolate regions of relatively clean sand, free of obvious mud deposits. Also shown in the figures are the x-coordinates of core samples

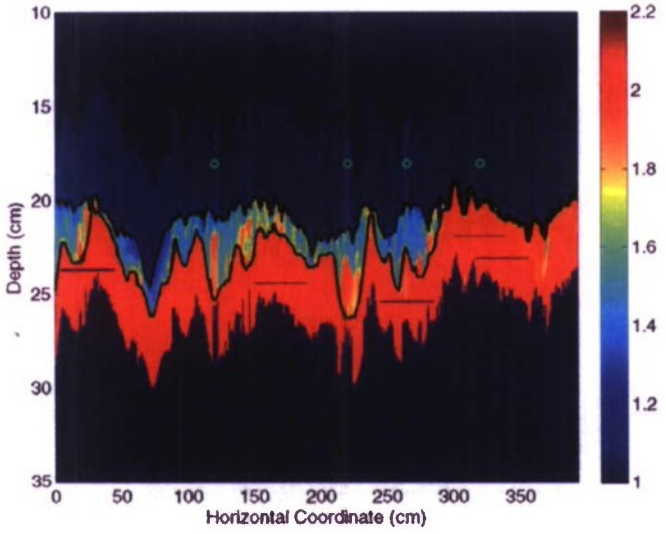

Fig. 6. Wet bulk density as determined from IMP2 run 118, oriented perpendicular to the ripple strike. There are no data for the highest and lowest dark blue regions. The horizontal blue lines indicate the data points used in analysis, and the green circles show the locations of diver cores. The seafloor and mud/sand interfaces are delineated by black curves. The color bar units are $kg \cdot m^{-3}$. Depth in the vertical axis is referenced to an arbitrary point on the IMP2 frame.

Fig. 7. Photograph of core FWB9-2 taken in conjunction with IMP2 run 117 at horizontal coordinate 273 cm. This location is marked by the third green circle from the left in Fig. 5. A mud layer occupies the top 4 cm of the core and contains a sand inclusion about 1 cm thick.

taken along the IMP2 sampling track. Four cores were taken for each of the two runs displayed, and these cores verified that the mud layers and sand pockets visible in the IMP2 data were correctly identified. A photograph of one of these cores is shown in Fig. 7 and can be compared with the IMP2 data of Fig. 5.

Figs. 5 and 6 clearly show that parts of the sandy bottom are covered by layers of mud as described earlier. In these mud layers, there are pockets of suspended sand. From an acoustic backscatter point of view, these sand inclusions might contribute significantly to high-frequency backscatter. Because we have only limited data, it is difficult to estimate the contribution these sand lenses have to acoustic backscattering. Such a calculation would require the size distribution of sand lenses including their frequency of occurrence per unit area. In addition, it would be necessary to model the gradation of acoustic properties of these pockets, which apparently do not always have sharp edges.

C. CT Data

The diver core shown in Fig. 8(a), collected from the sediment from which a conductivity measurement (run 117 at 303 cm) was made on October 4, 2004, was scanned with the Naval Research Laboratory (NRL) CT imager on May 23, 2006. During storage the core retained the seawater collected with the core and the macroscopic, physical properties of the sandy portion of the core were essentially the same as those present at the time of collection. The bulk density of the sample ranged from $1100\ kg \cdot m^{-3}$ at the top of the core to $2160\ kg \cdot m^{-3}$ at the conclusion of the CT scan at about 7.6-cm core depth. There is an obvious contrast between the lower density mud lying on top of the higher density sand at the bottom of the core [Fig. 8(b)]. It is important for interpretation of the bulk density fluctuations to realize that the interfaces between the overlying water and the mud surface, as well as between the mud and the sand surfaces, are not planar or perfectly aligned with the X-ray beams. Thus, determination of the bulk density within each thin disk of the low-resolution CT data (3.9-cm diameter, 95-μm thickness) results in the averaging of densities of water and mud or densities of mud and sand at these interfaces.

Within the low-density values averaging about $1200\ kg \cdot m^{-3}$ in the upper portion of the core, there are higher values peaking at 1700 and $1530\ kg \cdot m^{-3}$, probably due to sand lenses within the mud layer [Fig. 8(b)]. The presence of sand lenses at 0.8 and 1.5 cm from the sediment–water interface within the mud is consistent with the image in Fig. 8(a). Both within the mud layer and the underlying sand, the bulk density values show a gradual, but definite, increase with increasing depth in the core, in accordance with other fine-scale measurements in sand [13]. This slight increase in bulk density may be due to consolidation and dewatering via slow percolation of interstitial water through the bottom of the core during storage (an interval of 19 months between collection and scanning). However, as the surface elevation of the sand core that was evaluated by CT did not change noticeably during this period, it is unlikely that settling of sediments is the primary cause of this discrepancy. Also within the mud and sand data are small $250\text{-}kg \cdot m^{-3}$ fluctuations in bulk density.

The IMP2 profiles shown in Fig. 8(b) are taken from five adjacent vertical lines chosen to correspond to the position of the core shown in Fig. 8(a). There is considerable variation between the five density profiles in the mud layer. The values of density obtained from IMP2 in the mud layer are not correct, as the calibration discussed above only applies in sand.

D. Discussion of Sediment Heterogeneity

The sediment physical and acoustic properties at the SAX04 site exhibit relatively low variability when considering only the sand sediment (Table II). In terms of the CV, the sand sediment exhibits about half the variability in sound speed, porosity, bulk density, and mean grain size and similar variability in sound attenuation of that found in medium sands in coastal waters

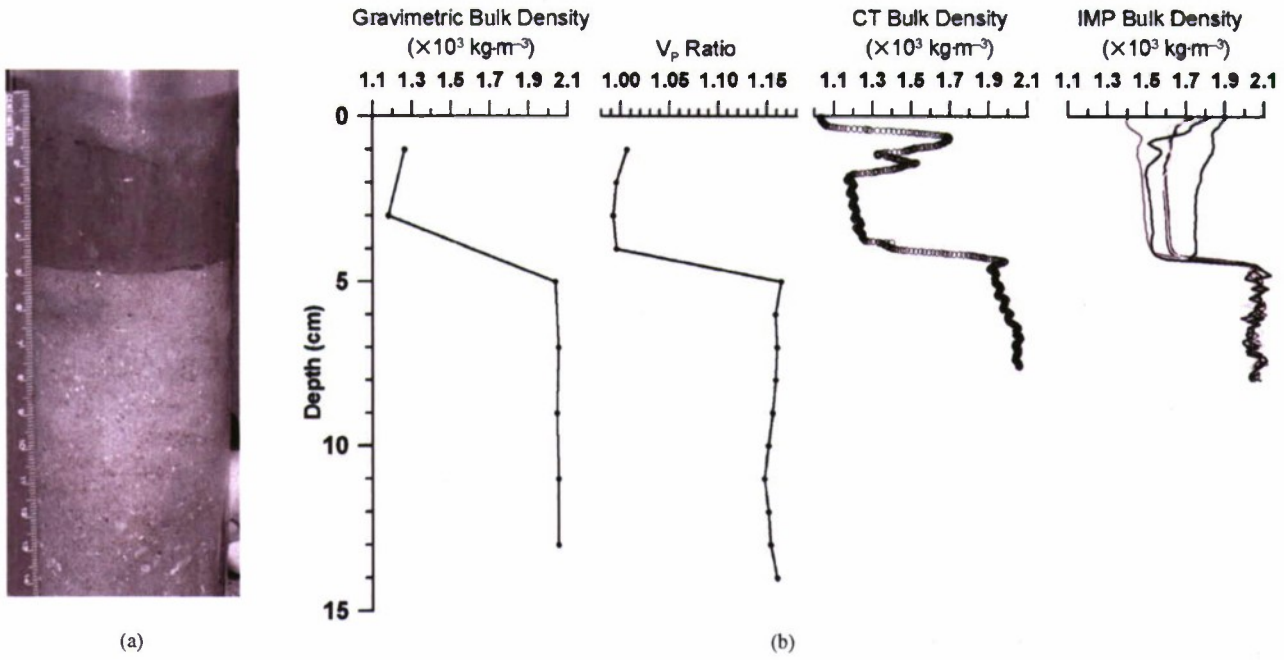

Fig. 8. (a) Photograph of the top 14 cm of core FWB9-1 collected from the site of IMP2 run 117 at horizontal coordinate 303 cm in Fig. 5. Sand lenses are visible near the surface of the 4-cm-thick mud layer. (b) Comparison of gravimetric bulk density, V_P ratio, and CT-derived bulk density measured from diver core FWB9-1 and IMP2 formation factor at IMP2 run 117 at 303 cm. The diver core was collected from the point of insertion of the IMP2 probe.

of similar depth [3, App. C]. Because 90% of the measurements of sediment sound speed were accomplished in sand (only 7% were made in mud/sand mixtures; 2.5% were made in pure mud), we will focus on fluctuations of sediment properties in the sand. Examining the sand data exclusive of any mud deposits from the 11 locations within the experiment site reveals that the area was relatively uniform. Furthermore, because the core sampling occurred over a period of six weeks, we can consider the properties of sand in this area to have little temporal change within the period of SAX04. Including the storm-deposited mud layers, flasers, and inclusions with the medium sand, however, boosts the CV values for these five parameters to those indicative of multimodal grain size distributions and sand–silt–clays [3, Sec. 7.5]. Indeed, there were temporal changes in the overlying mud layer due to hydrodynamic influences that resulted in thinning, mixing of mud with sand, burial, and, ultimately, advection of the mud away from the experiment area. Because the presence of the storm mud on the sandy seafloor was an anomaly, we consider, for the sake of greatest applicability of our results, that the parameterization of heterogeneity for predicting the scattering of high-frequency sound should involve only the sand data that excludes the mud data. Hence, sediment heterogeneity presumed responsible for scattering of high-frequency sound penetrating the sediment–water interface would be the fluctuations in sediment bulk density and sound speed that are a function of variations in granular properties of the sand (packing and sorting) rather than mud inclusions.

E. Comments on Comparison of Data

Acoustic measurements were made on core FWB9-1 on October 4, 2004 and the core was sectioned to measure bulk density gravimetrically on April 4, 2007. Ideally, core FWB9-1 would have been scanned in the CT imager and subsequently sectioned immediately following the acoustic measurements. However, technical problems with the CT imager and the necessity of completing multiple scans of the core before results were deemed satisfactory for statistical comparison with the conductivity and gravimetric data delayed the irreversible and destructive core sectioning for conventional bulk density determinations. Despite the large time lag, the core appeared similar in properties to those evident at the time of collection: although some consolidation of the overlying mud was apparent, there was no change in the volume of the sand sediment that is the subject of the data comparison. Furthermore, no evidence of biogenic structures or pyrite formation due to anoxia was observed in the CT imagery, which might introduce artifacts unrelated to naturally occurring sediment heterogeneity.

The profiles of Fig. 8(b) depict the same mud-overlying-sand scenario, but at different resolutions. The gravimetric bulk density is measured in 2-cm segments, the sediment sound speed is measured every centimeter, the CT image is composed of 95-μm segments, and the *in situ* formation factor is sampled in 1-mm increments. The 20-fold increase in resolution from sectioned core to *in situ* probe measurement (and comparable increase in vertical resolution from sectioned core to averaged CT imagery) provides different scales of sediment structure. Clearly, the gravimetric bulk density and sediment acoustic measurements delineate only the presence of ~4-cm-thick mud layer on top of sand, whereas the CT-derived bulk density measurements reveal the presence of sand lenses in the mud layer as well as fine-scale laminations. To some extent, the IMP2 profiles also indicate some fine-scale structure within the mud and sand sediments. This is evident in the individual profiles plotted to the far right of Fig. 8(b).

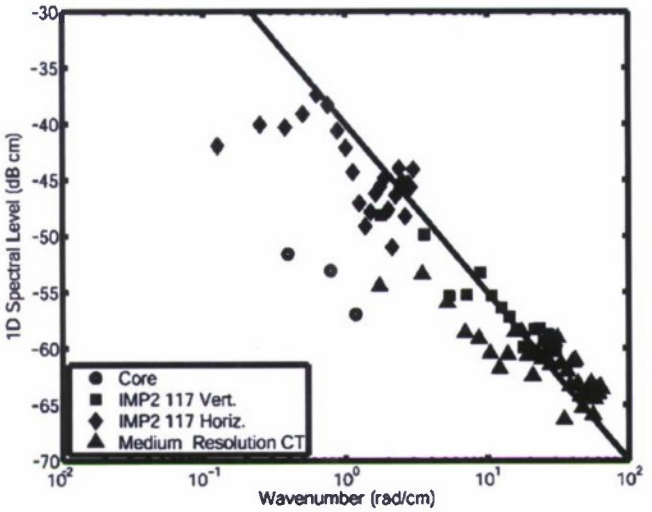

Fig. 9. One-dimensional spectra for normalized density fluctuations obtained by FFT from four data sources. The straight line corresponds to a 1-D spectral exponent of 1.5 or a 3-D exponent of 3.5.

IV. Statistical Characterization of Sediment Heterogeneity

In treating both sound-speed and density fluctuations, the fluctuating quantity will be taken as the difference from the mean divided by the mean. These random variables appear naturally in volume scattering models and will be referred to as "normalized" fluctuations. As is often done in the literature, sediment heterogeneity will be assumed to be isotropic, in part because the vertical measurements from cores provide only 1-D fluctuations for the estimates of covariance and the power spectrum. It has been demonstrated that horizontal scales of heterogeneity can be 1.5–10 times [14], [15] vertical scales of heterogeneity, and care must be exercised in comparison of data sampled in the vertical and horizontal dimensions. However, it should be noted that such anisotropy tends only to be visible at rather large spatial scales and was not observed at scales of order 10 cm and smaller in the work of Pouliquen and Lyons [16].

Power spectra characterizing spatial fluctuations in sound speed and density are often obtained using Fourier methods. This approach is most useful when rather long spatial series are available. In the present context, core sampling results in short series, having length of order 10 resolved samples. As a starting point in illustrating this and other issues encountered in the present work, Fig. 9 compares 1-D fast Fourier transform (FFT) power spectra for normalized density fluctuations obtained using core, IMP2, and medium-resolution averaged CT data (these are the CT data averaged over volumes comparable to the IMP2 resolution volume). With one exception, these spectra were obtained using a raised-cosine window (Hann window) to reduce leakage of the lower wave number parts of the spectra into the higher wave number parts. The core data series were so short that windowing was not applied. Even without windowing the core spectra have very little extent in wave number, seriously diminishing the usefulness of the FFT method. Another issue is the data smoothing caused by the necessary sectioning of core samples, with section length equal to the sampling interval. This amounts to a lowpass filtering operation with the filter rolloff frequency close to the sampling frequency. This causes a reduction in the high-wave-number content of the sampled data and a consequent bias in the power spectrum. The final issue of concern is the lack of agreement seen in Fig. 9 between spectra determined from differing data sources.

A method is developed in the Appendix to compensate for bias due to finite resolution, facilitating the comparison of data obtained by different methods. Another motivation for this method is the large quantity of historical core data. Even though the data series from a single core may be short, it seems reasonable to hope that, if multiple cores are available at a given site, useful estimates of heterogeneity spectra should be possible. This problem has previously been addressed by use of the autoregressive method [8], [14], [17], which employs a two-parameter model and estimates these parameters from the variance and unit-lag covariance of the data. The method used here and described in the Appendix is similar, but uses a three-parameter model and obtains these parameters by an approximate fit to small-lag values of the covariance. One element of the present method that has no counterpart in the autoregressive method is the use of the model to compensate for bias caused by the finite resolution of the sampling procedure. The method requires analysis to be restricted to a set of data series of a single length. In the case of sound-speed analysis, the length of the series corresponded to a maximum depth of 14 cm, and cores shorter than this were rejected. For density, the maximum depth was 16 cm. The method is also applied to the higher resolution IMP2 data, with the data restricted to a few "lines" of equal length with the lines being either horizontal or vertical.

The resolution-compensation method involves two steps. In the first step, the covariance of the measured normalized fluctuation is determined directly from a second moment of the data. This estimation is free of the problems associated with spectral leakage in the FFT method. In the second step, a synthetic biased covariance is generated assuming that the true power spectrum is of the "von Karman" form

$$W(\mathbf{k}) = \frac{w_3}{\left(k_x^2 + k_y^2 + \frac{k_z^2}{\Lambda^2} + L_0^{-2}\right)^{\gamma_3/2}} \tag{4}$$

where $\mathbf{k}$ is the 3-D wave vector having magnitude k. The four parameters of the spectrum are the "spectral strength" w_3, the "spectral exponent" γ_3, the "cutoff length" L_0, and the "anisotropy parameter" Λ. These parameters are varied until a reasonable match is obtained between the measured and synthetic biased covariances. For the core and IMP2 data, the anisotropy parameter was set to unity, as the data series are 1-D and estimation of anisotropy is not feasible. For the CT data, 3-D series are available, and the anisotropy parameter was adjusted as part of the fitting process.

Setting $\Lambda = 1$ yields a three-parameter model and implies that the fluctuations are statistically isotropic. This is expected to be a reasonable approximation at the scales of interest, 10 cm and smaller. In the case $\gamma_3 = 4$, the spectrum corresponds to the exponential covariance of the first-order autoregressive

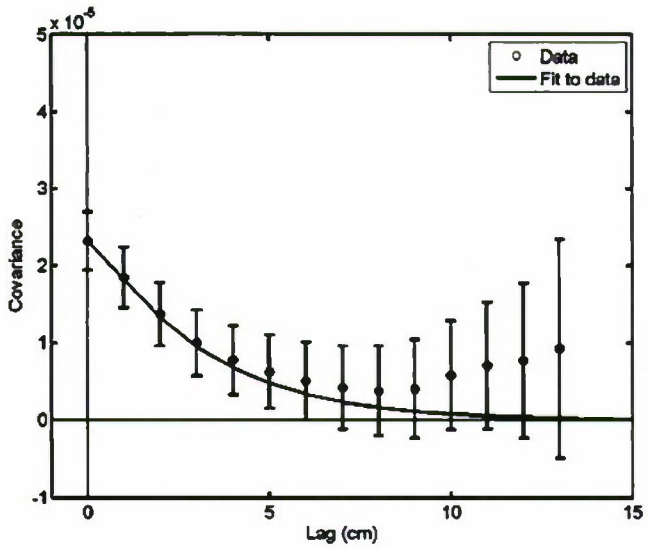

Fig. 10. Measured covariance of normalized sound-speed fluctuations (fluctuation about mean divided by mean) from 27 mud-free cores of length 14 cm and longer. The model for biased covariance fits the first several data points quite closely.

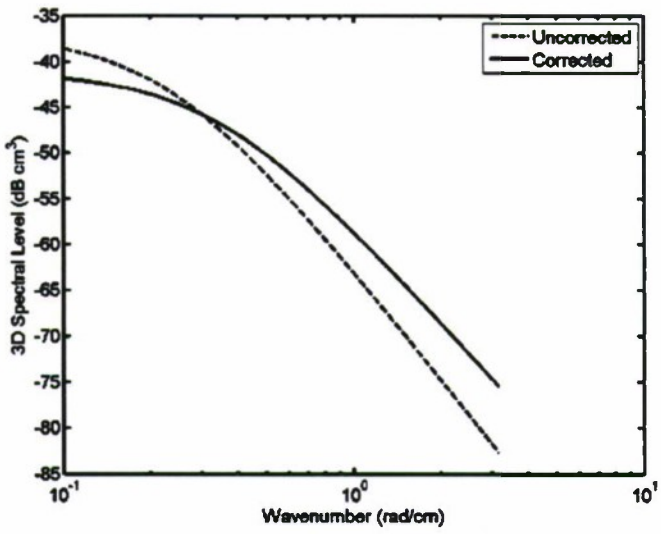

Fig. 11. Comparison of uncorrected and corrected spectra for sound-speed fluctuations. A set of 27 mud-free core samples was used. As a point of reference, a wave number of 1 cm^{-1} corresponds to an acoustic frequency of about 14 kHz in backscattering.

model, and L_0 then corresponds to the correlation length. The von Karman form has one more adjustable parameter, with values of γ_3 less than four providing greater high-frequency content. In treating both sound-speed and density fluctuations, the fluctuating quantity is taken as the difference from the mean divided by the mean. Because the fluctuating quantity is dimensionless, the spectrum has dimensions $(\text{length})^3$, thus w_3 has dimensions $(\text{length})^{(3-\gamma_3)}$. In the following, centimeter units will be used. In choosing the three spectral parameters that match the data, it has been found that there is considerable ambiguity in the choice of spectral exponent and cutoff length. Reasonable fits to the data considered here have been obtained with γ_3 in the range 3.1–4.0, with L_0 subsequently adjusted to provide a fit to the data. This is a shortcoming of the present trial-and-error method that might be eliminated if a more objective procedure were used. It has been found, though, that fits to the core and IMP2 data result in similar spectral parameters if γ_3 is assigned a midrange value $\gamma_3 = 3.5$. For the high-resolution CT data, the value $\gamma_3 = 3.2$ was found to give a noticeably better fit than the value 3.5. The straight line in Fig. 9 corresponds to a pure power law with $\gamma_3 = 3.5$ and with infinite L_0. Substantially different choices of γ_3 do not necessarily imply large differences in spectra if attention is restricted to the Nyquist band set by the sampling interval.

A. Core Data

Fig. 10 shows the covariance of normalized sound-speed fluctuations determined using 27 mud-free cores. Covariance and associated error bars were estimated using the methods defined in the Appendix. Also shown in the figure is a model fit for the case $\gamma_3 = 3.5$. The parameters obtained from the fit are given in the first row of Table III. The standard deviation of the estimate of the zero-lag covariance can be translated into a standard deviation of the estimate of w_3, amounting to 16% of the given value. With the present trial-and-error method, uncertainties are not obtained for γ_3 and L_0. The square root of the zero-lag covariance is the normalized standard deviation; multiplication by 100 gives the coefficient of variation, 0.48% in the present case. The measured CV differs slightly from the value 0.53% of Table II because of the cutting required to produce a data set having identical extent in depth. The bias correction yields a CV of 0.78%. To illustrate the effect of bias corrections on predictions for sediment volume scattering, heterogeneity spectra are displayed in Fig. 11 using the parameters obtained from covariance fitting with and without bias correction. The curves displayed in the figure are obtained by evaluating the 3-D spectral form (4) for different choices of spectral parameters. The curve labeled "uncorrected" was computed from a fit to the measured covariance using $\gamma_3 = 4.0$, $w_3 = 5.38 \times 10^{-7}$ cm^{-1}, and $L_0 = 4.37$ cm. This fit is representative of the result that would be obtained from first-order autoregressive analysis. The curve labeled "corrected" was computed using the parameters from the first row of Table III. In first-order perturbation theory, the scattering cross section is proportional to the spectrum evaluated at the Bragg wave number, so comparisons of the two spectra translate directly into comparisons of predicted scattering strength. For example, a wave number of 1 cm^{-1} corresponds to an acoustic frequency of about 14 kHz (for backscattering), and the corrected spectrum is about 4 dB higher than the uncorrected spectrum at this point. The correction becomes greater as frequency increases and *vice versa*.

A separate analysis was performed on a subset of four cores in close proximity to the SAX04 synthetic-aperture sonar rail system operated by the Applied Physics Laboratory (University of Washington, Seattle) with results given in Table III. These cores are of particular interest in modeling acoustic backscattering measured using this system [18] and are also of interest because they are in close proximity to the site of the conductivity data to be discussed below. The fit gives $L_0 = 1.0$ cm, considerably smaller than the value 3.0 cm obtained from the larger set of 27 mud-free cores. The measured CV is 0.33%,

TABLE III
HETEROGENEITY PARAMETERS DETERMINED FOR MUD-FREE SAMPLES USING DIFFERING DATA SOURCES. THE SPECTRAL EXPONENT IS $\gamma_3 = 3.5$ AND THE ANISOTROPY PARAMETER IS $\Lambda = 1$ FOR ALL DATA EXCEPT THE CT DATA, FOR WHICH $\gamma_3 = 3.2$ AND $\Lambda = 0.6$

	CV Uncorrected (%)	CV Corrected (%)	Cutoff Length, L_0 (cm)	Spectral Strength, w_3 ($cm^{-0.5}$)	Standard Deviation of Spectral Strength (%)
Sound Speed (27 Cores)	0.48	0.78	3.0	1.61×10^{-6}	16
Sound Speed (4 Cores)	0.33	0.80	1.0	2.94×10^{-6}	54
Bulk Density (6 Cores)	0.84	4.0	0.75	8.25×10^{-5}	26
Bulk Density (4 Cores)	0.44	1.65	1.0	1.24×10^{-5}	38
IMP2 (117 Horizontal)	1.82	2.32	1.0	2.44×10^{-5}	21
IMP2 (117 Vertical)	1.50	2.67	0.2	7.27×10^{-5}	11
CT	3.6	—	0.25	1.19×10^{-4}	4

somewhat smaller than that of the larger collection of mud-free cores, and the CV corrected for bias is 0.80% (Table III). These same four cores (and two others from other locations) were analyzed gravimetrically to determine wet bulk density, as will be discussed next.

The analysis of bulk density heterogeneity follows the same general approach as for sound speed, although the numerical algorithm for bias correction differs substantially. This is because the averaging volumes involved in the two types of measurement are different in shape. Again, the fluctuations are taken to be normalized and the underlying spectrum is assumed to be of the form (4). Fig. 12 compares the measured covariance obtained from six mud-free cores with the fitted spectral parameters given in the third row of Table III. The CV of the measured data from these six cores is 0.84%, to be compared with the value 0.59% from the 23 cores in Table II. These values differ owing to the data cutting required by the model fitting process. The bias-corrected CV is 4.0%. In contrast to the case of sound speed, bias correction has resulted in a large increase in the coefficient of variation. When the four mud-free cores near the rail system are analyzed, the result (fourth line of Table III) is a CV of 0.44% which is corrected to 1.65%. The corresponding spectral parameters have been altered to a considerable extent by the removal of two of six cores (compare the third and fourth rows of Table III). The model-data covariance fit for the four-core subset is not shown for purposes of economy, but the primary difference is in the smaller CV for the four-core subset. It was not possible to find a single fit that remained within the error bars for both cases, as the separation of the two estimated zero-lag covariances was about 2.5 standard deviations. For the four-core subset, both density and sound speed data have been fitted using the same spectral exponent and cutoff length. The fact that this is possible indicates that these two fluctuations have similar statistics, as assumed in most sediment volume scattering models.

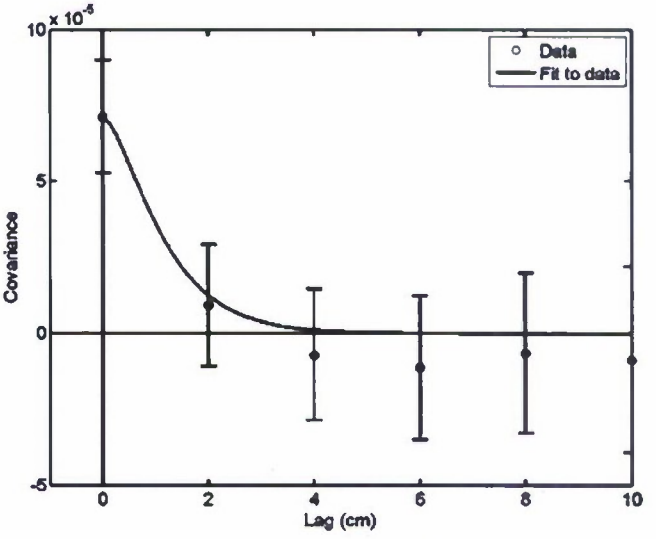

Fig. 12. Measured covariance of normalized wet bulk density fluctuations (fluctuation about mean divided by mean) from six mud-free cores of length 16 cm and longer compared to the model for biased covariance.

The difference between the results for the six- and four-core data subsets indicates that fluctuation properties have spatial variability that may not be apparent in average properties such as grain size, sound speed, and density.

B. *Conductivity Probe Data*

The IMP2 data displayed in Figs. 5 and 6 were analyzed in essentially the same manner as the core data, but with bias correction appropriate to the spherical symmetry of the sampling volume as discussed in the Appendix. The horizontal and vertical lines indicating samples to be analyzed were chosen to avoid obvious mud deposits. Because the conductivity probe

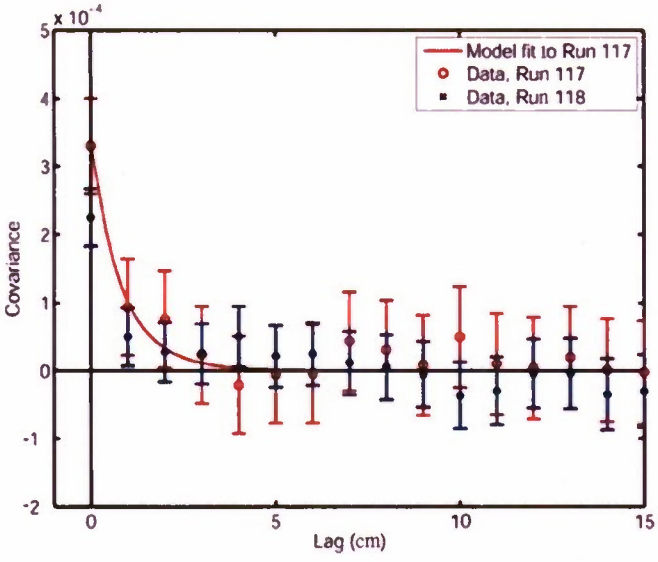

Fig. 13. Measured covariance of normalized wet bulk density fluctuations (fluctuation about mean divided by mean) from horizontally sampled IMP2 run 117 (parallel to ripple strike) compared to the model for biased covariance. Data from run 118 (perpendicular to ripple strike) are shown for comparison.

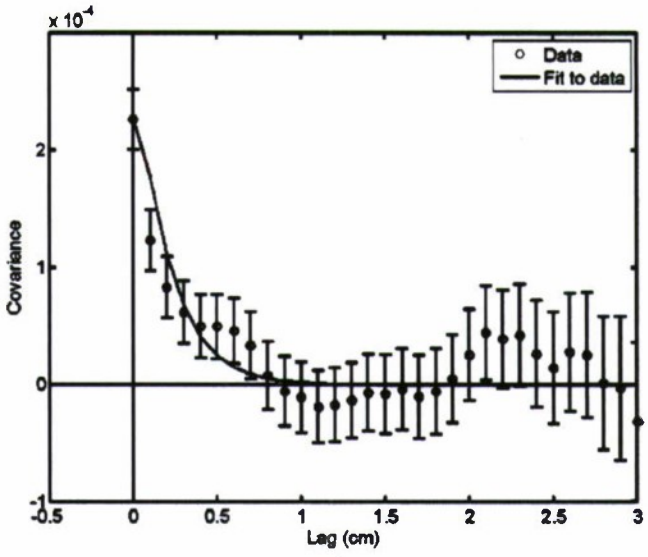

Fig. 14. Comparison of measured and modeled CT and vertical IMP2 covariance of normalized sediment bulk density fluctuations (fluctuation about mean divided by mean). The smooth curve is generated using the spectral parameters obtained by fitting the IMP2 data.

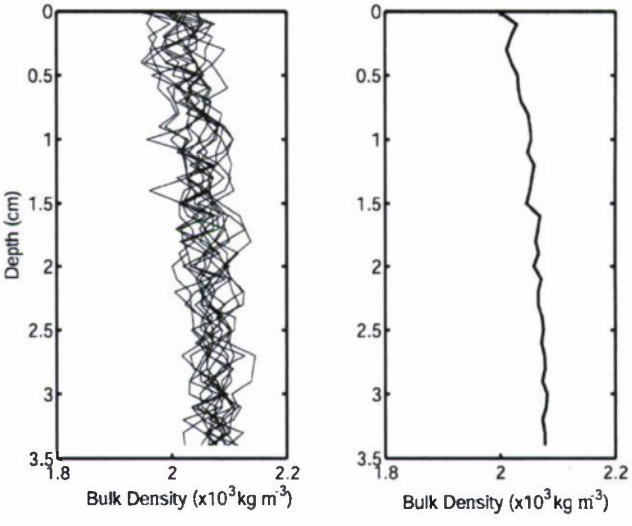

Fig. 15. Wet bulk density versus depth as determined from IMP2 run 117, with the individual profiles (see short vertical lines in Fig. 5) shown in the left-hand panel and the average of these shown in the right-hand panel.

is small, bias due to finite sampling volume is correspondingly smaller than for core analysis. Fig. 13 shows the covariance determined from a single IMP2 run (117) at the SJ (*R/V Seward Johnson*) location using the data indicated by horizontal lines in Fig. 5. This figure also shows a fit obtained using the model for biased covariance. Rather than attempting a complete fit, two of the model parameters were set to the values used in the four-core density case ($\gamma_3 = 3.5$ and $L_0 = 1.0$ cm). The resulting spectral parameters are given in the fifth row of Table III. The uncorrected CV is 1.82% and the corrected value is 2.32%. The IMP2 and four-core data were taken in the same vicinity near the rail system, so it is reasonable to compare the estimated spectral parameters for the two different measurements. First, it is significant that the same values of γ_3 and L_0 can be used in both cases with the model covariance remaining well within error bars. While the choice of γ_3 is arbitrary to some extent as noted above, once this choice is made the fit is sensitive to the subsequent choice of L_0. The estimated value for w_3 is about two times larger for the IMP2 data than for the core data. Although this may not seem to be a good match, it can be regarded as a partial success for the bias-removal method, as the uncorrected CVs would imply a factor of 17 between the two values of w_3, assuming all other spectral parameters are equal.

Similar results are obtained from IMP2 run 118 at the SJ location. The model curve that fits the data from run 117 provides a reasonable match to the estimated covariance for run 118, as can be seen in Fig. 13. These two IMP2 runs were taken at essentially the same location, with the sampling direction for run 117 oriented parallel to the dominant sand ripple strike and the sampling direction for run 118 oriented perpendicular to the strike.

The results given above were obtained with sampling of IMP2 data along the horizontal lines of Figs. 5 and 6. When the data from the vertical lines in Fig. 5 are analyzed, the covariance is markedly different. The measured covariance and the model fit are shown in Fig. 14. The most striking difference (compare fifth and sixth rows of Table III) is in the small value for the parameter L_0, which indicates that the vertical heterogeneity has structure on scales of 1 mm, but lacks centimeter-scale structure. Inspection of Fig. 5 suggests a reason for this difference. The vertical sampling lines in the figure follow in their vertical placement the up-and-down undulations of the sediment–water interface. As a result, a depth-dependent trend in density appears identically in all vertical data series, as is evident in Fig. 15. This trend is subtracted by the mean removal used in processing (Appendix). In contrast, the horizontally sampled data will exhibit longer scale fluctuations because the horizontal lines cut through this trend as it undulates vertically. This results in variation in the horizontal data on scales comparable to those of the interface undulations,

i.e., centimeter scales. One may then ask why the vertically sampled core data did not also yield a small value for L_0, but the cores have approximately four times greater vertical extent than the vertical IMP2 lines, so the lower frequency content of the core data should be greater.

C. CT Data

Spatial covariance of normalized sediment bulk density fluctuations was estimated for the high-resolution CT data. As noted earlier, these data comprised eight profile sets, each set consisting of a 10×10 array of adjacent vertical profiles. One of the original nine profile sets was discarded as it displayed a trend with depth differing strongly from the other eight. Covariance was estimated in both vertical and horizontal directions. For the analysis of covariance in the vertical, eight single profiles were taken from the approximate center of each set. The analysis of these profiles was similar to those conducted with the core- and IMP2-derived data discussed above except that, after subtracting the depth-dependent mean, the separate profiles displayed offsets, such that each profile had a significantly different average value. To accommodate this characteristic, another subtraction was performed, removing the profile mean from each profile. In estimating horizontal covariance, the estimate employed all 800 high-resolution profiles, with lags taken in only one of the two possible directions. Error bars were not computed for the horizontal data, but should be smaller than those for the vertical data owing to the employment of a larger data set. The estimated horizontal and vertical covariances are shown in Fig. 16. It is apparent that the horizontal covariance falls off more rapidly with increasing lag than the vertical covariance. This is more likely due to differing CT resolution in the two directions than to anisotropy of the medium.

Analysis of the high-resolution CT data employed a significantly different strategy than that used for core and IMP2 data. Owing to the high resolution of the CT data and lack of knowledge of the appropriate averaging volume, no bias corrections were made. Instead, spectral parameters were obtained by fitting the uncorrected theoretical covariance to the data of Fig. 16, with the anisotropy parameter allowed to vary. There is no contradiction with the earlier assertion that the medium is likely to be isotropic at the small scales of interest, as the spectrum is taken as a model for the data as biased by differing horizontal and vertical resolutions, and these data are apparently anisotropic. The parameters obtained from the fit are $\gamma_3 = 3.2$, $w_3 = 1.19 \times 10^{-4}$ cm^{-1}, $L_0 = 0.025$ cm, and $\Lambda = 0.6$, and the CV is 3.6%. The standard deviation of w_3 is 4.0%.

To facilitate comparison with IMP2, the CT data were averaged over volumes 0.5 mm $\times$ 0.5 mm in the horizontal and 0.475 mm in the vertical, to approximate the sampling volume of IMP2. As noted earlier, these averaged data will be referred to as "medium-resolution CT data." The dimensions of the individual sampling volumes comprising the averaged profiles constructed from the CT imagery are only a little larger than the mean grain diameter (0.363 mm). Fig. 17 compares the estimated covariance for the medium-resolution CT data with model curves. The CT-derived model curve fits the data rather well, both in level and width. This fit was seriously degraded when anisotropy was ignored by employing only vertical high-resolution covariance data. This example is not an inversion as in previous cases, because the underlying statistics of the high-resolution CT data were already determined in the model-fitting exercise above. Rather, this example should be considered as a validation of the bias-removal algorithm for the case of a well-understood (rectangular) averaging volume. When spectral parameters obtained from the IMP2 data in the vertical are used in the model, the resulting covariance is in clear disagreement. This is because the IMP2 data are richer in low spatial frequencies as evidenced by their larger cutoff length (0.2 cm versus 0.025 cm).

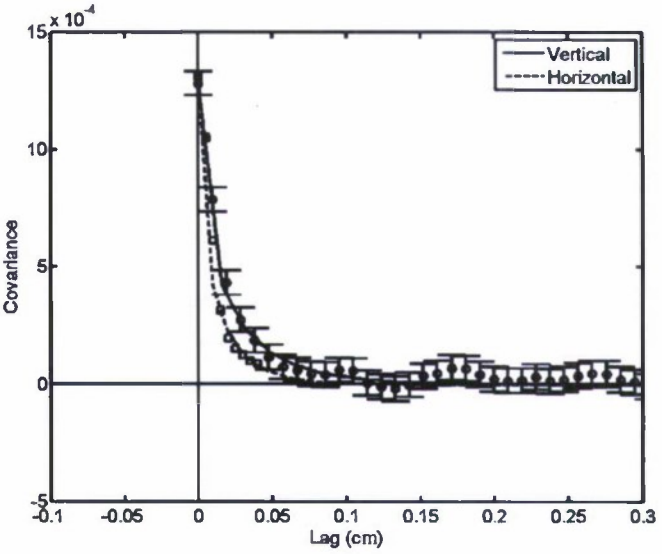

Fig. 16. Comparison of measured and modeled CT covariance of normalized sediment bulk density fluctuations in the vertical and horizontal directions. The smooth curves are generated by adjusting the parameters of the spectrum (4) for a simultaneous fit to both vertical and horizontal covariances.

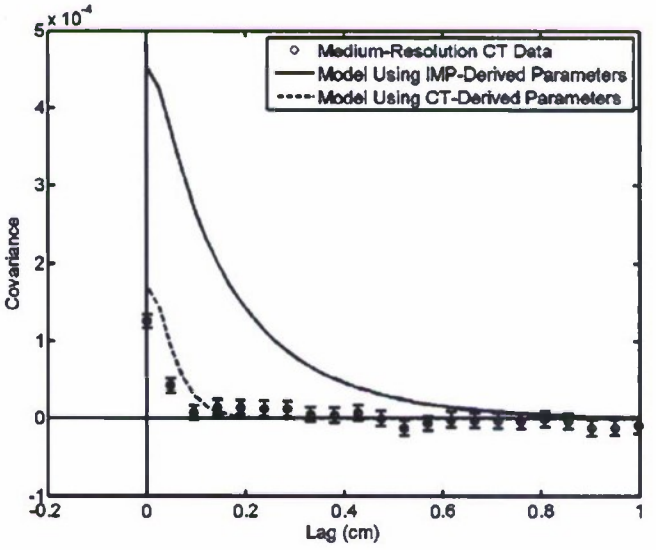

Fig. 17. Comparison of measured and modeled medium-resolution CT covariance (CT data averaged over contiguous volumes to mimic IMP2 resolution). The model curves are generated using spectral parameters obtained by fitting the IMP2 data and the high-resolution CT data.

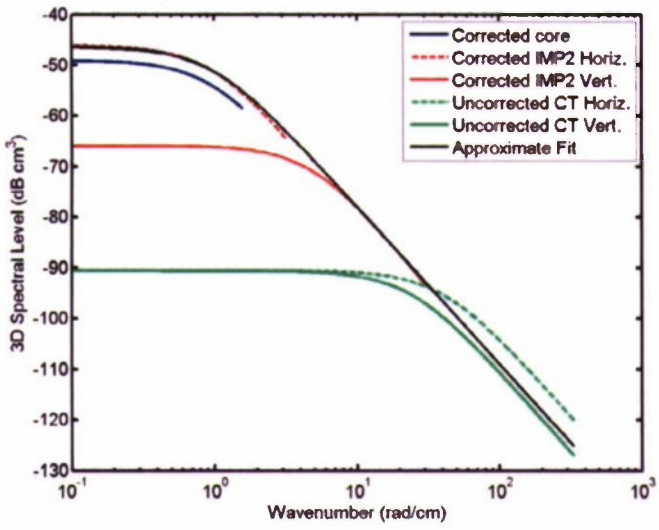

Fig. 18. Comparison of 3-D spectra for normalized density fluctuations as determined from four mud-free core samples, IMP2 data, and high-resolution CT data. These spectra are obtained from (4) using parameters given in the text, and with the curves terminated at the Nyquist frequency appropriate to each measurement method. The solid black curve is an "eyeball" fit to the spectra, ignoring the rolloff of the IMP2 vertical and CT spectra.

D. Comparison of Spectra

The spectral parameters derived from the various data sources are diverse, but a comparison of the corrected spectra shows a striking regularity. The curves shown in Fig. 18 are smooth because they have been computed using (4) with parameters from the text. All spectra are plotted over wave numbers up to the Nyquist limit, which is π divided by the sampling interval. It is apparent that the high-frequency asymptotes of the spectra align quite well. This suggests that the data represent a single overall spectrum such as that shown by the solid black curve in Fig. 18. The parameters for this spectrum are $\gamma_3 = 3.1$, $w_3 = 2.0 \times 10^{-5}$ cm$^{-0.1}$, and $L_0 = 1.05$ cm. The wave number at which the various spectra roll off is determined by the cutoff length L_0. For the longest data series (core and IMP2 horizontal), the cutoff length has a stable value of about 1 cm, essentially the same value used in the fit for the overall spectrum. This appears to be an intrinsic value, part of the statistical characterization for scales up to the longest series (1 m for the horizontal IMP2 data). The IMP2 vertical and CT series have short lengths, about 3.5 cm, and their cutoff lengths are much shorter than 1 cm. As explained earlier, the necessary tactic of taking the IMP2 vertical profiles in a fashion that conforms to the undulations of the water–sediment interface resulted in "erasure" of features having scales on the order of 1 cm and accounts for the small cutoff length (0.2 cm). The even smaller cutoff length (0.025 cm) of the CT data is a result of two factors: the extreme horizontal localization of the data (near the center of a single core) and the subtraction of the mean profile in the covariance estimation process. As the separate profiles contributing to the estimate are separated by horizontal distances of about 1 cm, a good deal of small structure will be lost in the subtraction. Within the limitations of the various measurement methods, and after correction for sampling bias, the data sets appear to be consistent and to indicate that the normalized density fluctuations can be characterized by the overall spectrum defined above.

V. Summary

As resolution of the sediment heterogeneity is changed from 2-cm increments to much smaller separations between measurements, the nature of the heterogeneity changes. When examining changes in sediment conductivity separated by 1 mm, or changes in CT-derived sediment bulk density separated by 0.5 mm, fine-scale structure is apparent in the place of the relative uniformity seen from centimeter-scale measurements. It is the covariances and corresponding power spectra of these fine-scale fluctuations that are important quantities for models predicting acoustic scattering. In comparison of core, IMP2 and CT data having widely differing resolutions point toward a single, unifying spectrum for heterogeneity.

The method used to correct for bias due to finite spatial resolution appears to have been partially successful in reconciling heterogeneity measurements having widely differing resolutions. Considering measurements at the site of the IMP2 data reported here, the uncorrected core data showed a much smaller coefficient of variation (0.44%) than the uncorrected conductivity data (1.84%). Bias correction largely resolved this discrepancy, yielding corrected coefficients of variation of 1.65% and 2.34% for the core and conductivity data, respectively. Bias correction allowed fitting of core-derived sound-speed and density data by a single spectral shape, differing only in strength. Further development of this method is warranted, with a particular need for objective means of fitting the model to data and obtaining measures of uncertainty. The largest core data set analyzed for bias correction comprised 15 depth samples in 27 cores, a total of 405 samples. As only three spectral parameters are to be estimated, it seems that uncertainty might not be as large as that obtained by admitting all fits within the error bars in Fig. 10. Either Bayesian or maximum-likelihood approaches may be suitable, although these would require extensive numerical computation. Either approach could assume underlying Gaussian statistics, and the model covariances determining all relevant statistical properties would be computed as in the present work and used to form the likelihood function.

Appendix

We provide here details on the methods used to estimate heterogeneity spectra and associated errors from core and conductivity measurements. Core data and vertical IMP2 lines were treated in the same fashion, while horizontal IMP2 lines and CT data were each treated with methods adapted to particular issues encountered in the estimation process. The measured sediment parameter (either bulk density or sound speed divided by an average value) will be denoted x_{mn}, where m is an index denoting core or line number and n is an index denoting the sample number within a core or line. For core data and vertical IMP2

lines, a depth-dependent sample mean and a depth-independent covariance are formed as follows:

$$\mu_n = \frac{1}{M}\sum_{m=1}^{M} x_{mn} \tag{5}$$

$$K_p = \frac{1}{(M-1)(N-p)} \times \sum_{m=1}^{M}\sum_{n=1}^{N-p}(x_{mn}-\mu_n)(x_{mn-p}-\mu_{n-p}). \tag{6}$$

The sample index n takes on N values, where N is either the number of samples available in the shortest core admitted for analysis or the number of samples in an IMP2 vertical line. Although the mean is allowed to be depth dependent, it is inherent in (6) that fluctuations about this mean are assumed stationary with respect to depth. The lag index p ranges from 0 to $N-1$, but statistical error increases as p increases owing to the decreasing number of samples contributing to the sum on n. The denominator factor in (6) ensures that K_p is an unbiased estimator of the covariance.

The finite spatial resolution of the various measurement techniques introduces bias in the estimate of heterogeneity spectra. To counteract this bias, the following approach is used. First, it is assumed that the true spectrum is of the form (4) to preserve short wavelength features that might be lost by using Gaussian or exponential forms. Next, the method of [3, Sec. 7.4] is used to obtain the biased covariance corresponding to (4), accounting for the finite resolution of the core measurement process which is treated as a 3-D filtering operation. For example, when density is measured by weighing core sections, the cylindrical "disk" shape of the sample defines the filter impulse response, constant within the sample and zero outside. The measured data are assumed to be the true data convolved with this impulse response. In [3, eq. (D.53)], the resultant biased vertical heterogeneity spectrum is given. In the present work, this theoretical biased spectrum is formed, and then a Fourier transform is used to obtain the theoretical biased vertical covariance. This theoretical covariance is compared with the sample covariance, and the parameters of (4) are adjusted until a satisfactory fit is found. This fit is presently achieved by trial-and-error rather than by either maximum-likelihood or Bayesian schemes.

In the case of sound-speed measurements on cores, the sample shape is not a disk; rather it is a diffused shape extending horizontally across the core. As an idealization, the sample volume in this case is taken to be a line extending across the core diameter. The neglect of the finite breadth of the sound beam used in these measurements is not expected to cause significant error, as the largest dimension of the sampling volume is the primary determinant of bias. The steps in fitting spectra in this case differ from those used for density. First, the true 3-D covariance corresponding to (4) is found by means of a Fourier transform for a trial set of the three spectral parameters. Second, this covariance is convolved with the autocorrelation of the straight-line impulse response (a triangular function) to obtain the theoretical biased covariance. This process is repeated for other values of the spectral parameters until a suitable match between the theoretical and sample covariances is obtained.

The spectral bias due to the finite size of the spherical conductivity probe is found by multiplying (4) by [3, eq. (D.54)], and an inverse transform is used to obtain the biased covariance for comparison with the estimate (6). The sampling volume for medium-resolution CT data is a sharp-edged rectangular shape having side lengths $2a_h$ in the horizontal and $2a_v$ in the vertical. Equation (D.54) in [3] is replaced by

$$V(\mathbf{k}) = [\mathrm{sinc}(k_x a_h)\mathrm{sinc}(k_y a_h)\mathrm{sinc}(k_z a_v)]^2 \tag{7}$$

where $\mathrm{sinc}(x) = \sin(x)/x$, $a_h = 0.25$ mm, and $a_v = 0.2375$ mm.

For the conductivity probe, data sampled in the vertical are treated identically to core data. However, in horizontal sampling, the mean subtraction is handled differently. A single mean value is estimated for each of M horizontal lines ($M = 2$ in Fig. 5 and $M = 5$ in Fig. 6)

$$\mu_m = \frac{1}{N}\sum_{n=1}^{N} x_{mn}. \tag{8}$$

The covariance is then estimated as

$$K_p = \frac{1}{M(N-p)}\sum_{m=1}^{M}\sum_{n=1}^{N-p}(x_{mn}-\mu_m)(x_{mn-p}-\mu_m). \tag{9}$$

This estimator for covariance, unlike (6), is slightly biased, but calculations show that this lag-dependent bias is insignificant compared to statistical error owing to small sample size. The estimator used for both high- and medium-resolution CT data uses both mean subtractions, first subtracting a depth-dependent mean and then subtracting the mean for each separate vertical line. Expression (6) is used, and the lag-dependent bias is expected to be unimportant.

The error bars given for covariance estimates were computed under the assumption of Gaussian statistics. If each of the samples entering an estimate of the covariance were uncorrelated, the variance of the estimate (6) for lag index p, normalized by the square of the covariance, would be $2/N_{\mathrm{tot}}$, where N_{tot} is the normalizing integer appearing in the denominator of (6), that is, $N_{\mathrm{tot}} = (M-1)(N-p)$ for core processing, vertical IMP2 lines, and CT data. Of course, the samples are not uncorrelated, and the covariance provides an estimate of the sample-to-sample correlation within a given core or conductivity probe line. Under the Gaussian assumption, it can be shown that N_{tot} in the variance of the estimate is reduced by a factor equal to the sum of the squares of the true correlation over all lags. In computing error bars, the true correlation has been replaced by the estimated correlation, which is the estimated covariance divided by its zero-lag value. Denoting the estimated correlation $\rho(p)$,

N_{tot} in the estimate variance is reduced by division by the factor $b = \rho^2(0) + 2[\rho^2(1) + \rho^2(2) + \rho^2(3) + \cdots]$. The factor of two simply accounts for combination of terms having positive and negative lag. Finally, the standard deviation of the covariance estimate is computed as

$$\sigma_K = \sqrt{\frac{2b}{N_{\text{tot}}}} K_0 \tag{10}$$

where K_0 is the estimated covariance at zero lag. Error bars are given length $2\sigma_K$ and centered on the estimated covariance value. For processing of horizontal IMP2 lines, $N_{\text{tot}} = M(N - p)$ is used. For the IMP2 horizontal line data and the CT data, approximations are used that have not been examined in detail, but are expected to be more than adequate for estimates of error.

ACKNOWLEDGMENT

The authors would like to thank M. Welch, who was responsible for the design and construction of IMP2. They would also like to thank the captains and crews of the *R/V Pelican* and *R/V S. Johnson* for enabling deployment of IMP2 and many diving operations required to make SAX04 successful.

REFERENCES

[1] E. I. Thorsos, K. L. Williams, N. P. Chotiros, J. T. Christoff, K. W. Commander, C. F. Greenlaw, D. V. Holliday, D. R. Jackson, J. L. Lopes, D. E. McGehee, M. D. Richardson, J. E. Piper, and D. Tang, "An overview of SAX99: Acoustic measurements," *IEEE J. Ocean. Eng.*, vol. 26, no. 1, pp. 4–25, Jan. 2001.

[2] M. D. Richardson, K. B. Briggs, L. D. Bibee, P. A. Jumars, W. B. Sawyer, D. B. Albert, R. H. Bennett, T. K. Berger, M. J. Buckingham, N. P. Chotiros, P. H. Dahl, N. T. Dewitt, P. Fleischer, R. Flood, C. F. Greenlaw, D. V. Holliday, M. H. Hulbert, M. P. Hutnak, P. D. Jackson, J. S. Jaffe, H. P. Johnson, D. L. Lavoie, A. P. Lyons, C. S. Martens, D. E. McGehee, K. D. Moore, T. H. Orsi, J. N. Piper, R. I. Ray, A. H. Reed, R. F. L. Self, J. L. Schmidt, S. G. Schock, F. Simonet, R. D. Stoll, D. Tang, D. E. Thistle, E. I. Thorsos, D. J. Walter, and R. A. Wheatcroft, "An overview of SAX99: Environmental considerations," *IEEE J. Ocean. Eng.*, vol. 26, no. 1, pp. 26–54, Jan. 2001.

[3] D. R. Jackson and M. D. Richardson, *High-Frequency Seafloor Acoustics*. New York: Springer-Verlag, 2007.

[4] W. C. Vaughan, K. B. Briggs, J.-W. Kim, T. S. Bianchi, and R. W. Smith, "Storm-generated sediment distribution along the northwest Florida inner continental shelf," *IEEE J. Ocean. Eng.*, vol. 34, no. 4, pp. 495–515, Oct. 2009.

[5] H.-E. Reineck and I. B. Singh, *Depositional Sedimentary Environments*. New York: Springer-Verlag, 1980, pp. 112–114.

[6] D. Fan, C. Li, and P. Wang, "Influences of storm erosion and deposition on rhythmites of the Upper Wenchang formation (Upper Ordovician) around Tonglu, Zhejiang Province, China," *J. Sediment. Res.*, vol. 74, no. 4, pp. 527–536, 2004.

[7] K. B. Briggs and A. H. Reed, "Using CT to image storm-generated stratigraphy in sandy sediment off Fort Walton Beach, Florida, USA," in *Proc. Int. Conf. Underwater Acoust. Meas.: Technol. Results*, Heraklion, Crete, Greece, 2005, pp. 95–102.

[8] D. Tang, K. B. Briggs, K. L. Williams, D. R. Jackson, E. I. Thorsos, and D. B. Percival, "Fine-scale volume heterogeneity measurements in sand," *IEEE J. Ocean. Eng.*, vol. 27, no. 3, pp. 546–560, Jul. 2002.

[9] D. Tang, "Fine-scale measurements of sediment roughness and subbottom variability," *IEEE J. Ocean. Eng.*, vol. 29, no. 4, pp. 929–939, Oct. 2004.

[10] W. M. Telford, L. P. Geldart, R. E. Sheriff, and D. A. Keys, *Applied Geophysics*. Cambridge, U.K.: Cambridge Univ. Press, 1976, p. 775.

[11] G. E. Archie, "The electrical resistivity log as an aid in determining some reservoir characteristics," *Trans. AIME Petrol. Tech.*, vol. 146, no. 5, pp. 54–62, 1942.

[12] S. L. Wellington and H. J. Vinegar, "X-ray computerized tomography," *J. Petrol. Tech.*, vol. 39, no. 8, pp. 885–898, 1987.

[13] R. A. Wheatcroft, "*In situ* measurements of near-surface porosity in shallow-water marine sands," *IEEE J. Ocean. Eng.*, vol. 27, no. 3, pp. 561–570, Jul. 2002.

[14] K. B. Briggs and D. Tang, "Statistical variability of sediment sound speed and density in fine and medium sands," in *Proc. 5th Eur. Conf. Underwater Acoust.*, Lyon, France, 2000, pp. 1265–1270.

[15] T. Yamamoto, "Acoustic scattering in the ocean from velocity and density fluctuations in the sediments," *J. Acoust. Soc. Amer.*, vol. 99, pp. 866–869, 1996.

[16] E. Pouliquen and A. P. Lyons, "Backcattering from bioturbated sediments at very high frequency," *IEEE J. Ocean. Eng.*, vol. 27, no. 3, pp. 388–402, Jul. 2002.

[17] K. B. Briggs and D. B. Percival, "Vertical porosity and velocity fluctuations in shallow-water surficial sediments and their use in modeling volume scattering," in *High-Frequency Acoustics in Shallow Water*, N. G. Pace, E. Pouliquen, O. Bergem, and A. P. Lyons, Eds. La Spezia, Italy: NATO SACLANT Undersea Res. Ctr, 1997, pp. 65–73.

[18] K. L. Williams, E. I. Thorsos, D. Tang, D. R. Jackson, and K. B. Briggs, "Acoustic backscattering from a sand and a sand/mud environment: Experiments and data/model comparisons," *IEEE J. Ocean. Eng.*, vol. 34, no. 4, pp. 388–398, Oct. 2009.

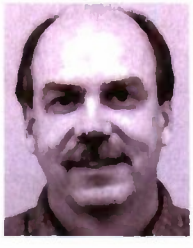

Kevin B. Briggs received the B.S. degree in biology from Florida Atlantic University, Boca Raton, in 1975, the M.S. degree in zoology from the University of Georgia, Athens, in 1978, and the Ph.D. degree in marine geology and geophysics from the Rosenstiel School of Marine and Atmospheric Science, University of Miami, Miami, FL, in 1994.

He began working at the Naval Ocean Research and Development Activity, now part of the Naval Research Laboratory (NRL), Stennis Space Center, MS, in 1979, where he was involved in research on the effects of environmental processes on sediment geoacoustic properties. He has participated in many shallow-water high-frequency acoustics experiments as an investigator of geoacoustic and roughness properties of the seafloor. He is currently engaged in research on characterization of sediment interface roughness and volume inhomogeneity for high-frequency acoustic modeling. He has over 40 published articles on physical and acoustic properties of the seafloor.

Dr. Briggs is a member of the Acoustical Society of America and the American Geophysical Union.

Allen H. Reed received the B.S. degree in oceanography from Humboldt State University, Arcata, CA, in 1996, the M.S. degree in marine science from The University of Southern Mississippi, Hattiesburg, in 1999, and the Ph.D. degree in coastal studies from the Louisiana State University, Baton Rouge, in 2004.

Currently, he is a Geologist focusing on marine sedimentology in the littoral and oceanic environments. His primary interest is in determining sediment physical properties, sediment fluid and thermal conductivities, and geotechnical properties. He has worked in the Seafloor Sciences Branch at the Naval Research Laboratory, Naval Space Center, MS, for 12 years. He has worked in the Baltic, the Beaufort Sea, off the coast of Brazil and in several coastal environments surrounding the continental United States.

Darrell R. Jackson received the B.S., M.S., and Ph.D. degrees in electrical engineering from the University of Washington, Seattle, in 1960, 1963, and 1966, respectively. His thesis research was directed toward applications of magnetic resonance. He received the Ph.D. degree in physics from California Institute of Technology (Caltech), Pasadena, in 1977, with a dissertation on the extraction of experimental predictions from quark-gluon theory.

He worked at Boeing as a Research Engineer. He was a faculty member at the University of Massachusetts, Amherst. Since joining the Applied Physics Laboratory (APL), University of Washington, in 1976, his research has centered on underwater acoustics. Sound scattering by the seafloor has been a dominant research topic, including inversions of scattering data for sensing of benthic activity. Since retirement in 2000, he has continued his research as a Senior Fellow at APL and coauthored the book *High-Frequency Seafloor Acoustics* with M. D. Richardson (New York: Springer-Verlag, 2006).

Dr. Jackson is a Fellow and Silver Medalist of the Acoustical Society of America.

Dajun Tang received the B.S. degree from University of Science and Technology, Hefei, China, in 1981, the M.S. degree from the Institute of Acoustics, Beijing, China, in 1985, and the Ph.D. degree in oceanographic engineering from the Joint Program of Massachusetts Institute of Technology and the Woods Hole Oceanographic Institution, Woods Hole, MA, in 1991.

From 1991 to 1996, he was first an Assistant Scientist and then Associate Scientist at Woods Hole Oceanographic Institution. In 1996, he moved to the Applied Physics Laboratory, University of Washington, Seattle, where he is currently a Senior Oceanographer. His primary research interest is ocean acoustics.